

Cite this: *Chem. Sci.*, 2018, 9, 6062

# Operando deconvolution of photovoltaic and electrocatalytic performance in ALD TiO<sub>2</sub> protected water splitting photocathodes†

Wei Cui,<sup>a</sup> Wenzhe Niu,<sup>ab</sup> René Wick-Joliat,<sup>a</sup> Thomas Moehl<sup>a</sup> and S. David Tilley<sup>a\*</sup>

In this work, we demonstrate that buried junction photocathodes featuring an ALD TiO<sub>2</sub> protective overlayer can be readily characterized using a variation of the dual working electrode (DWE) technique, where the second working electrode (WE2) is spatially isolated from the hydrogen-evolving active area. The measurement of the surface potential during operation enables the *operando* deconvolution of the photovoltaic and electrocatalytic performance of these photocathodes, by reconstructing  $J-\Delta V$  curves (reminiscent of photovoltaic  $J-V$  curves) from the 3-electrode water splitting data. Our method provides a clearer understanding of the photocathode degradation mechanism during stability tests, including loss of the catalyst from the surface, which is only possible in our isolated WE2 configuration. A  $\text{pn}^+\text{Si/TiO}_2$  photocathode was first investigated as a well behaved model system, and then the technique was applied to an emerging material system based on  $\text{Cu}_2\text{O/Ga}_2\text{O}_3$ , where we uncovered an intrinsic instability of the  $\text{Cu}_2\text{O/Ga}_2\text{O}_3$  junction (loss of photovoltage) during long term stability measurements.

Received 29th March 2018

Accepted 5th June 2018

DOI: 10.1039/c8sc01453a

rsc.li/chemical-science

## Introduction

Photoelectrochemical (PEC) water splitting has been recognized as a promising avenue for harvesting renewable hydrogen fuel from inexhaustible solar energy and water.<sup>1–4</sup> Large photovoltages are required for efficient and therefore cost-effective water splitting, and one approach to achieving larger open-circuit voltages ( $V_{\text{oc}}$ ) is using so-called “buried junctions”. These buried junction photoelectrodes can be modeled as a series combination of a p–n junction photoabsorber, a protective layer and surface catalyst (pn/cat),<sup>5,6</sup> where the  $V_{\text{oc}}$  is decoupled from the semiconductor–electrolyte interface, and the increased band bending of the p–n junction can significantly enhance electron–hole pair separation.<sup>7</sup>

The efficiency of a pn/cat photocathode is largely determined by the intrinsic properties of the buried p–n junction.<sup>8</sup> However, the semiconductor–catalyst and catalyst–electrolyte interfaces also play a critical role in the overall performance of the system. Issues such as charge transport in the protective layer, the nature of the semiconductor–catalyst contact (ohmic or Schottky-type), as well as the electrocatalytic activity at the catalyst–electrolyte interface are typically obscured within the standard current–

voltage measurement data.<sup>9,10</sup> Therefore, we sought to develop an experimental technique that could not only evaluate the PEC performance but also simultaneously provide an understanding of these different interfaces during PEC operation.

The dual working electrode (DWE) technique was first reported in the 1970s. Nakato, Pinson and Wilson reported that n-GaP and n-TiO<sub>2</sub> photoanodes coated with thin gold films showed a photovoltaic effect, representing early examples of *in situ* measurements of the surface potential.<sup>11–13</sup> Recently, the Boettcher group has used the DWE technique to study a photoanode–catalyst interface.<sup>14</sup> It is of note that the second working electrode in all of the previous works has either been a transparent conducting oxide (TCO) or a thin metal film that covers the entire active area.<sup>15,16</sup> For systems that do not employ TCOs as part of the buried junction structure, it has thus far not been possible to carry out DWE studies without introducing a metallic film, which influences the measurement through partial light absorption and by affecting the catalyst binding to the photoelectrode surface. We have therefore developed a new architecture of the DWE technique that is compatible with standard buried junction photocathodes featuring a protective layer, which does not introduce extraneous materials at the semiconductor–electrolyte interface. With this method, one can diagnose a problem of the stability of the catalyst on the surface *versus* the stability of the photovoltaic output of the p–n junction. As will be shown in this manuscript, the latter case does indeed require consideration. The diagnosis of the point of failure in unmodified PEC devices under operation is critical for identification of targets to improve the system.

<sup>a</sup>Department of Chemistry, University of Zurich, Winterthurerstrasse 190, CH-8057 Zurich, Switzerland. E-mail: david.tilley@chem.uzh.ch

<sup>b</sup>State Key Laboratory of Silicon Materials, School of Materials Science and Engineering, Zhejiang University, Hangzhou, Zhejiang, China

† Electronic supplementary information (ESI) available: SEM images, Faradaic efficiencies,  $V_2/\Delta V-V_1$  curve, etc. See DOI: 10.1039/c8sc01453a



A TiO<sub>2</sub>-protected pn<sup>+</sup>-Si junction photocathode was chosen as a platform to develop this method, as the Si p-n junction is robust and stable. Atomic layer deposition (ALD) TiO<sub>2</sub> is a common protective layer for water splitting photocathodes due to its favorable conduction band position for the hydrogen evolution reaction, optical transmittance for visible light, high stability over a wide range of electrolyte solutions and pH, and good conductivity. Moreover, the high doping density of ALD TiO<sub>2</sub> enables an ohmic (tunnel) contact to the contacting metal of the second working electrode (WE2), no matter the work function.<sup>17,18</sup> The top contact was made *via* a thin Au layer covered by epoxy, which was able to sense the surface potential of the photocathode under *operando* conditions, without directly contacting the electrolyte or HER catalyst. The hidden *J*-*V* curve of the buried p-n junction can then be extracted by measuring the difference in voltage between the backside and the surface of the photocathode ( $\Delta V$ ) and plotting *versus* the water splitting current. By monitoring the evolution of the hidden *J*-*V* curve in the 3-electrode water splitting measurements, one can immediately diagnose whether the degradation in the performance of the photocathode derives from a problem with the catalyst or with the photovoltaic output of the p-n junction. In this work, we evaluate both a well understood system (pn<sup>+</sup>-Si) and a promising emerging system (p-n Cu<sub>2</sub>O/Ga<sub>2</sub>O<sub>3</sub>). The results from the Si system demonstrate that the failure of the surface catalyst is easily identified with our DWE technique. The results from the Cu<sub>2</sub>O-based system reveal an intrinsic instability of the p-n junction, with reduced photovoltaic output following a stability measurement.

## Results and discussion

### Interface energetics of the pn<sup>+</sup>Si/TiO<sub>2</sub>/Pt(ed) photocathode

A pn<sup>+</sup>-Si photocathode with 100 nm-thick ALD-TiO<sub>2</sub> protective layer was chosen as a model system for the development of the technique. A schematic diagram of the DWE setup is depicted in Fig. 1a. WE1 is used for controlling the back contact potential (*V*<sub>1</sub>) of the photocathode. WE2 is connected to the photocathode surface and kept at open circuit during PEC measurements to directly probe the surface potential (or in other words to probe the energy level of surface-accumulated electrons) in relation to the reference electrode (*V*<sub>2</sub>). To avoid direct contact of WE2 and the active area, WE2 was contacted a small distance away from the illuminated area (~1 mm) and separated by a thin coating of opaque epoxy, as shown in Fig. 1b. When illuminated, electron-hole pairs are generated and separated by the built-in electric field across the p-n junction, bringing photoelectrons to the surface while sweeping holes to the back contact. Consequently, a photovoltage is created across the pn<sup>+</sup>-Si homojunction. Considering that both the n-type Si layer and TiO<sub>2</sub> are highly doped,<sup>19</sup> the width of the space charge region of both n<sup>+</sup>-Si and TiO<sub>2</sub> is very narrow and ensures an Ohmic contact. The Pt catalyst also forms an Ohmic contact with the TiO<sub>2</sub> layer.<sup>17</sup> As a result, the measured potentials of *V*<sub>1</sub> and *V*<sub>2</sub> directly give the energetic positions of the quasi-Fermi level of holes and electrons, respectively. The difference between *V*<sub>1</sub> and *V*<sub>2</sub>, denoted  $\Delta V$ , is the output voltage of the pn<sup>+</sup>-Si junction. It is

worth noting that as the photoelectrons diffuse away from the illuminated area (as shown in Fig. 1b), the electrons cannot enter the electrolyte and will ultimately recombine. This leads to a lower electron density than in the illuminated area and a slightly reduced *V*<sub>oc</sub> compared to the photovoltaic output of the p-n junction is recorded. The small drop in the measured surface potential is robust and reproducible, and does not complicate the analysis herein.

After the Pt catalyst was electrodeposited onto the TiO<sub>2</sub> surface, the conventional current density-back contact potential (*J*-*V*<sub>1</sub>) curve of the pn<sup>+</sup>Si/TiO<sub>2</sub>/Pt(ed) photocathode was obtained in 0.5 M H<sub>2</sub>SO<sub>4</sub> with a linear sweep from positive to negative potential (Fig. 1c). Under one sun illumination, the pn<sup>+</sup>Si/TiO<sub>2</sub>/Pt(ed) photocathode exhibits an onset potential for water reduction of ~0.5 *V*<sub>RHE</sub>. As *V*<sub>1</sub> becomes more negative, the photocurrent density increases and eventually saturates at 25 mA cm<sup>-2</sup> at *V*<sub>1</sub> = -0.2 *V*<sub>RHE</sub>. WE2 enables the *in situ* measurement of surface potential *V*<sub>2</sub> during the sweep of *V*<sub>1</sub>. ESI Fig. S3† presents *V*<sub>2</sub> and  $\Delta V$  values as a function of *V*<sub>1</sub> with and without illumination.

A hidden *J*- $\Delta V$  curve, analogous to the current-voltage characteristic of a PV cell, can then be extracted and is plotted in Fig. 1c. The *V*<sub>oc</sub> and *J*<sub>sc</sub> are 475 mV and 24.6 mA cm<sup>-2</sup>, respectively (the characteristics are also listed in ESI Table S1†). A significant loss of fill factor is observed when comparing the *J*-*V*<sub>1</sub> and *J*- $\Delta V$  curves, which derives from the additional series resistances in a PEC cell *versus* a PV cell, namely the TiO<sub>2</sub>/catalyst junction resistance, the overpotential of the catalyst required for driving a chemical reaction, and the solution resistance.<sup>20</sup> In essence, the *J*- $\Delta V$  curve shows the best possible fill factor that can be achieved by the *J*-*V*<sub>1</sub> curve. In practice, a real PEC *J*-*V*<sub>1</sub> curve will always have a smaller fill factor due to the catalyst overpotential as well as the series resistances mentioned above.

In order to more clearly visualize the effect of the surface potential on the current, a stepwise chronoamperometry measurement was carried out whereby the potential of *V*<sub>1</sub> was stepped every 30 s and both *V*<sub>2</sub> and the photocurrent were recorded (Fig. 1d). When *V*<sub>1</sub> is positive of ~0.5 *V*<sub>RHE</sub> (and the photocurrent is still nearly 0), *V*<sub>2</sub> remains at a constant distance (constant  $\Delta V$ , see also ESI Fig. S3†). Substantial cathodic photocurrents appear at *V*<sub>1</sub> = 0.4 *V*<sub>RHE</sub>, where *V*<sub>2</sub> is (due to the photovoltage) more negative than 0 *V*<sub>RHE</sub> (with  $\Delta V$  now starting to shrink). After the onset potential, although *V*<sub>2</sub> continues to move negatively with each step,  $\Delta V$  shrinks further as the photocurrent increases. Ultimately, both *V*<sub>2</sub> and the photocurrent become constant, even as *V*<sub>1</sub> becomes more negative, eventually entering a reverse bias-type regime. ESI Fig. S4† depicts band energy diagrams under several conditions of applied bias, and ESI Fig. S5† gives a detailed discussion of the relationship between photovoltage and the onset potential.

### Stability of the pn<sup>+</sup>Si/TiO<sub>2</sub>/Pt(ed) photocathode

A critical issue for photoelectrodes is the long-term stability. A standard procedure for assessing the stability is to carry out a chronoamperometry experiment under a static back contact





**Fig. 1** Schematic illustration of (a) the DWE configuration used during PEC measurements with a  $\text{pn}^+\text{Si}/\text{TiO}_2/\text{Pt}$  photocathode and (b) the structure of the sensing electrode WE2, located a small distance ( $\sim 1$  mm) away from the illuminated area, separated by a thin coating of opaque epoxy (not to scale). For simplicity, the band bendings at the interfaces of the highly doped  $\text{n}^+\text{-Si}$  and  $\text{TiO}_2$  have been omitted. (c) The  $J$ - $V_1$  and  $J$ - $\Delta V$  curves of  $\text{pn}^+\text{Si}/\text{TiO}_2/\text{Pt}(\text{ed})$ , collected by a LSV scan toward negative potential with a scan rate of  $10 \text{ mV s}^{-1}$  in  $0.5 \text{ M H}_2\text{SO}_4$ .  $\Delta V = V_1 - V_2$ . (d)  $V_2$  and  $J$  values of  $\text{pn}^+\text{Si}/\text{TiO}_2/\text{Pt}(\text{ed})$  with stepwise controlled  $V_1$  under illumination. Each  $V_1$  step lasts 30 s.  $\text{Pt}(\text{ed})$  indicates that the Pt was deposited by electrodeposition.

potential and to compare the  $J$ - $V_1$  behavior before and after the stability test. This type of analysis, however, is relatively limited because the underlying degradation mechanisms are inaccessible. The decrease in PEC performance can be due to several factors. Firstly, the  $\text{H}_2$ -evolving catalyst may be deactivated, poisoned or dislodged from the electrode surface. Secondly, the p-n junction may produce a reduced output  $V_{\text{oc}}$ , due to partial photocorrosion and increased recombination. These changes in the semiconductor material also result in lower photocurrent densities and fill factor.

In order to characterize the degradation mechanism in the Si photocathode, we performed a 2 h stability test by holding  $V_1$  at  $0 V_{\text{RHE}}$ , a typical value for these types of test in the literature.<sup>8</sup> Fig. 2a shows the  $J$ - $V_1$  and  $J$ - $\Delta V$  curves before and after the 2 h stability test. Compared with the initial  $J$ - $V_1$  scan, the scan after the 2 h shows similar onset potential and slightly decreased saturation photocurrent, but a remarkably poorer fill factor. As the  $J$ - $\Delta V$  curves remain the same, it is immediately apparent that the problem relates to the catalyst and not to the photovoltaic performance of the buried junction. Fig. 2b depicts how the surface potential  $V_2$  and photocurrent density change over time under a static back contact potential of  $0 V_{\text{RHE}}$ . Over 2 h, the photocurrent density drops from  $\sim 23$  to  $\sim 20 \text{ mA cm}^{-2}$ , while  $V_2$  steadily shifts to more negative values, which indicates that higher overpotential is needed in order to achieve a similar current density. A poor contact between the surface and the catalyst ( $\text{TiO}_2/\text{catalyst}$ ) as well as worsening kinetics at the

catalyst/electrolyte interface (*e.g.* surface poisoning) will result in a higher overpotential for the catalytic interface.<sup>21</sup> Pt was then re-deposited onto the electrode surface (Fig. 2c). Due to the fact that the fill factor is completely restored upon re-platinization, we can confirm that neither a degradation in the p-n junction of the silicon nor resistive losses through *e.g.* formation of a silicon oxide layer are responsible for the change in the  $J$ - $V_1$  curve. The degradation likely results from desorption of the Pt nanoparticles, as has been previously observed for electrodeposited platinum on ALD  $\text{TiO}_2$ .<sup>22</sup> When the ALD  $\text{TiO}_2$  was replaced by a thin metallic Ti film, the Pt catalyst binding was much more robust over a 2 h stability measurement (ESI Fig. S7†)

### Investigation of the $\text{TiO}_2/\text{Pt}$ junction

For the  $\text{pn}^+\text{-Si}$  photocathodes described above, the Pt catalyst was electrodeposited onto either the  $\text{TiO}_2$  or Ti metal surface as nanoparticles with a size range of  $\sim 10$ – $30 \text{ nm}$  (ESI Fig. S8a†). This non-continuous catalyst morphology may be unfavorable for efficient extraction of the surface electrons, resulting in a poor fill factor of the  $J$ - $V_1$  curve.<sup>23</sup> Therefore, we investigated a nominally 2 nm-thick Pt film with nearly full coverage on the  $\text{TiO}_2$  layer by sputter coating (denoted  $\text{pn}^+\text{Si}/\text{TiO}_2/\text{Pt}(\text{sp})$ ). The Pt deposited in this way makes the surface slightly rough (ESI Fig. S8b†). Fig. 3a compares the  $J$ - $V_1$  curves of  $\text{pn}^+\text{Si}/\text{TiO}_2/\text{Pt}(\text{sp})$  and  $\text{pn}^+\text{Si}/\text{TiO}_2/\text{Pt}(\text{ed})$  photocathodes under one sun illumination. Sputtered Pt exhibits a similar onset potential and improved fill factor, but



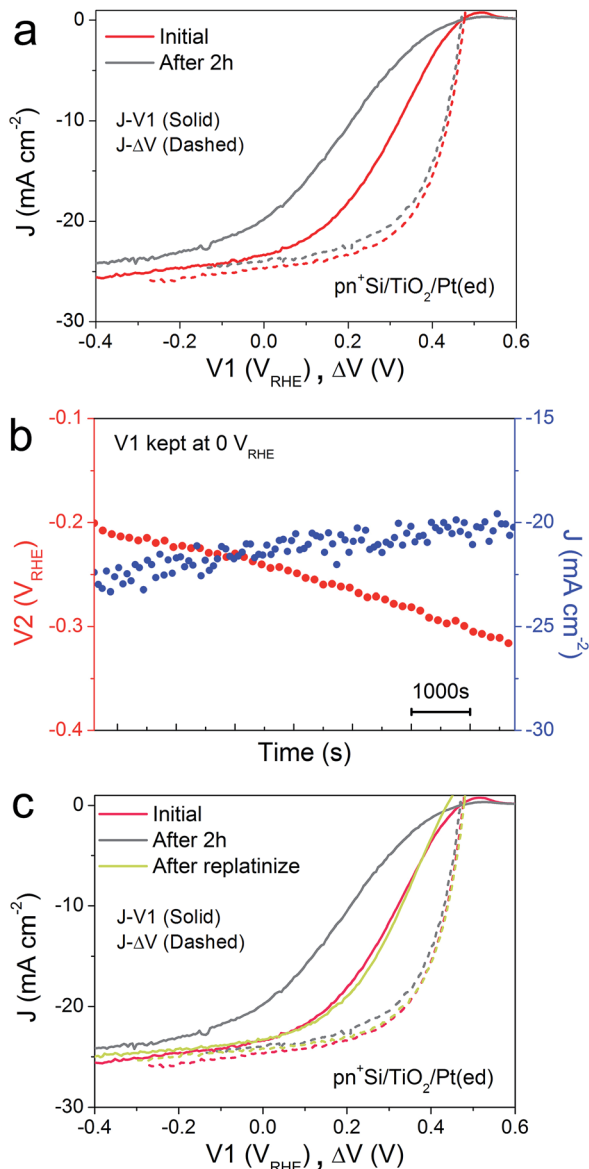


Fig. 2 (a)  $J$ - $V_1$  (solid) and  $J$ - $\Delta V$  curves (dashed) of  $\text{pn}^+\text{Si}/\text{TiO}_2/\text{Pt}(\text{ed})$  before and after a 2 h stability test, collected by a LSV scan with a scan rate of  $50 \text{ mV s}^{-1}$  towards negative potential in  $0.5 \text{ M H}_2\text{SO}_4$ . (b) Changes in  $V_2$  and  $J$  during a 2 h stability test.  $V_1$  is held at  $0 V_{\text{RHE}}$ . (c)  $J$ - $\Delta V$  curves (dashed) of  $\text{pn}^+\text{Si}/\text{TiO}_2/\text{Pt}(\text{ed})$  and the corresponding  $J$ - $V_1$  curves (solid). All data are collected under simulated one sun illumination.

much reduced photocurrent densities due to the optical transmission loss through the 2 nm-thick Pt film (ESI Fig S9<sup>†</sup>). For better comparison between the sputtered and electrodeposited samples, we also measured the  $J$ - $V_1$  curve of the  $\text{pn}^+\text{Si}/\text{TiO}_2/\text{Pt}(\text{sp})$  at an increased light intensity to achieve a similar photocurrent density, plotted in green. The green curve exhibits an earlier onset potential despite having the same  $V_{\text{oc}}$  as the  $\text{Pt}(\text{ed})$  curve, suggesting a better catalytic activity of sputtered Pt over electrodeposited Pt. Support for this hypothesis is shown by comparing their individual catalytic activities towards  $\text{H}_2$  generation when deposited on FTO slides (Fig S10<sup>†</sup>). Additionally,  $\text{pn}^+\text{Si}/\text{TiO}_2/\text{Pt}(\text{sp})$  always shows an enhancement in the fill factor

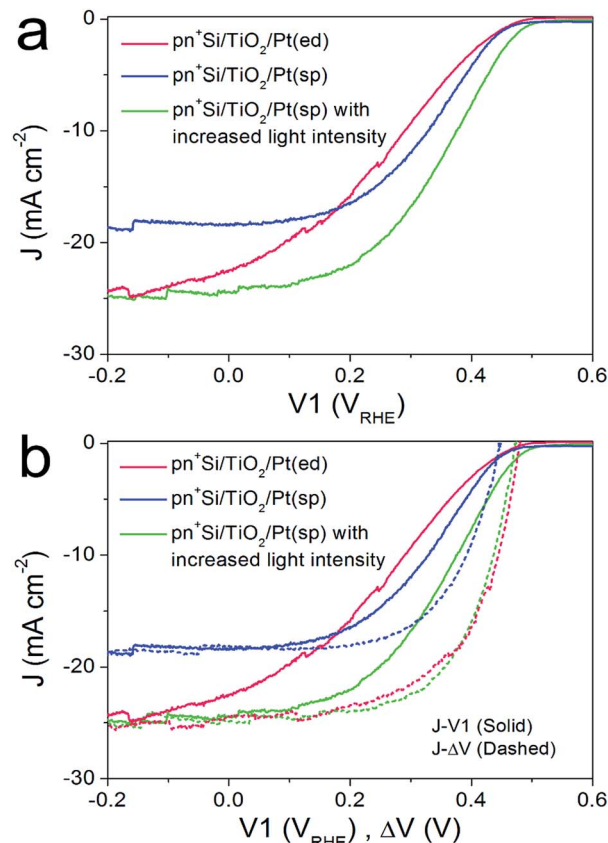


Fig. 3 (a) Comparison of  $J$ - $V_1$  curves between  $\text{pn}^+\text{Si}/\text{TiO}_2/\text{Pt}(\text{ed})$  and  $\text{pn}^+\text{Si}/\text{TiO}_2/\text{Pt}(\text{sp})$ , collected by a LSV scan with a scan rate of  $10 \text{ mV s}^{-1}$  towards negative potential in  $0.5 \text{ M H}_2\text{SO}_4$ . (b)  $J$ - $\Delta V$  curves (dashed) of  $\text{pn}^+\text{Si}/\text{TiO}_2/\text{Pt}(\text{ed})$  and  $\text{pn}^+\text{Si}/\text{TiO}_2/\text{Pt}(\text{sp})$ , combined with their  $J$ - $V_1$  curves (solid). All data are collected under illumination. For comparison, the performance of  $\text{pn}^+\text{Si}/\text{TiO}_2/\text{Pt}(\text{sp})$  with similar photocurrent densities as  $\text{pn}^+\text{Si}/\text{TiO}_2/\text{Pt}(\text{ed})$ , by increasing the light intensity, is also displayed (green solid and dashed curves).

the in  $J$ - $V_1$  curves, reflecting the smaller  $\text{TiO}_2/\text{Pt}$ /electrolyte interfacial resistance for the  $\text{TiO}_2/\text{Pt}(\text{sp})$  as compared to the  $\text{TiO}_2/\text{Pt}(\text{ed})$ . In the case of a conformal Pt film, electron transfer is more probable as the catalyst surface area is increased, which is also indicated by the much more positive  $V_2$  value in  $\text{pn}^+\text{Si}/\text{TiO}_2/\text{Pt}(\text{sp})$ , shown in ESI Fig. S11<sup>†</sup>. For example, to reach the same saturation photocurrent, a  $\sim 130 \text{ mV}$  overpotential is required for  $\text{pn}^+\text{Si}/\text{TiO}_2/\text{Pt}(\text{sp})$  but  $\sim 200 \text{ mV}$  for  $\text{pn}^+\text{Si}/\text{TiO}_2/\text{Pt}(\text{ed})$ .

What we have already hypothesized by the performance of the different Pt on FTO is confirmed by the determination of the  $J$ - $\Delta V$  curves. At similar saturation photocurrents the  $J$ - $\Delta V$  (PV mode) of  $\text{pn}^+\text{Si}/\text{TiO}_2/\text{Pt}(\text{sp})$  is essentially identical with the  $\text{pn}^+\text{Si}/\text{TiO}_2/\text{Pt}(\text{ed})$  (see the green and red dashed curves) while the  $J$ - $V_1$  curve (PEC mode) shows a clearly higher FF for the device with sputtered Pt.

### $\text{Cu}_2\text{O}/\text{Ga}_2\text{O}_3$ junction photocathode

Thus far, we have developed the DWE technique with a model  $\text{pn}^+\text{Si}/\text{TiO}_2/\text{Pt}(\text{ed})$  photocathode, with which we can gain a deeper insight into the PEC process and the photocathode





stability. Next, we applied this technique to the emerging material ALD  $\text{TiO}_2$ -protected  $\text{Cu}_2\text{O}$  to demonstrate the generality of the technique and to probe a potential instability of the photovoltaic output of these materials.<sup>22,24</sup> An n-type  $\text{Ga}_2\text{O}_3$  was used as a buffer layer between the  $\text{Cu}_2\text{O}$  and  $\text{TiO}_2$  overlayer because this interlayer ensures a positively shifted onset potential, compared to that of n-Al:ZnO (AZO) (ESI Fig. S12†).<sup>25,26</sup> Fig. 4a schematically depicts the multilayer structure of the  $\text{Cu}_2\text{O}/\text{Ga}_2\text{O}_3/\text{TiO}_2$  photocathode. In a similar fashion as for the silicon photocathodes described previously, a second working electrode was introduced to probe the surface potential  $V_2$ , prior to deposition of the Pt catalyst by sputtering.

PEC measurements were performed in a pH 5 phosphate/sulfate solution. Fig. 4b displays the  $J$ - $V_1$  and  $J$ - $\Delta V$  curves. A positive onset potential of  $\sim 0.9 V_{\text{RHE}}$  is observed in the  $J$ - $V_1$  curve, and at  $V_1 = 0 V_{\text{RHE}}$ , the photocurrent density is  $3.9 \text{ mA cm}^{-2}$ . The onset potential is much more positive than that from both  $\text{Cu}_2\text{O}/\text{ZnO}$  and  $\text{Cu}_2\text{O}/\text{AZO}$  photocathodes, reflecting the larger photovoltage generated by the  $\text{Cu}_2\text{O}/\text{Ga}_2\text{O}_3$  junction. In the case of the  $J$ - $\Delta V$  curve, the  $V_{\text{oc}}$ ,  $J_{\text{sc}}$  and fill factor are 836 mV,  $4.0 \text{ mA cm}^{-2}$  and 36.1%, respectively. Compared with reported  $\text{Cu}_2\text{O}/\text{Ga}_2\text{O}_3$  solar

cells in the literature, the  $V_{\text{oc}}$  and fill factor values are comparable, but the  $J_{\text{sc}}$  is lower due to light absorption by the Pt catalyst.<sup>26,27</sup> Still, resistance at the  $\text{TiO}_2/\text{Pt}/\text{electrolyte}$  interfaces contribute to the fill factor loss between the  $J$ - $V_1$  and  $J$ - $\Delta V$  curves. The fill factor loss is not very significant. As the  $J$ - $\Delta V$  curve mirrors the  $J$ - $V_1$  curve, it is clear that the photovoltaic output of the buried  $\text{Cu}_2\text{O}/\text{Ga}_2\text{O}_3$  junction is responsible for the shape of the  $J$ - $V_1$  curve of the photocathode, and not the catalytic activity of the Pt catalyst. When using an electrodeposited Pt catalyst the PEC system exhibits a lower fill factor, indicating that the  $\text{TiO}_2/\text{Pt}/\text{electrolyte}$  resistance indeed can also limit  $J$ - $V_1$  performance, as shown in ESI Fig. S15.† We further carried out a stepwise test on the photocathode under illumination. Results and discussion are provided in ESI Fig. S16 and S17† and confirm our statements above.

To study the stability of the  $\text{Cu}_2\text{O}/\text{Ga}_2\text{O}_3/\text{TiO}_2/\text{Pt}(\text{sp})$  photocathode, a 2 h chronoamperometric measurement was performed under illumination at  $V_1 = 0 V_{\text{RHE}}$ . Fig. 4b shows the comparison of the  $J$ - $V_1$  curves before and after a 2 h stability test. The onset potential shows a negative shift of nearly 120 mV, although the photocurrent density remains similar. Fig. 4b also shows the initial  $J$ - $\Delta V$  curve and the one after the 2 h stability test. An obvious decrease in  $V_{\text{oc}}$  is evident, from 836 mV to 743 mV, while the  $J_{\text{sc}}$  shows a slight increase from 4.0 to  $4.1 \text{ mA cm}^{-2}$  (ESI Table S1†). In contrast to the  $\text{pn}^+\text{-Si}$  photocathode, the  $\text{Cu}_2\text{O}/\text{Ga}_2\text{O}_3$  photocathode shows a degradation of the photovoltaic output of the underlying buried junction. For the silicon system,  $J$ - $\Delta V$  remained constant while the  $J$ - $V_1$  changed (Fig. 2). For the  $\text{Cu}_2\text{O}/\text{Ga}_2\text{O}_3$  case,  $J$ - $\Delta V$  has changed while  $J$ - $V_1$  remains similar (retains a similar photocurrent and fill factor). In order to determine the origin of the degraded photovoltage, a solid-state measurement was carried out using the DWE photocathode in a 2-electrode configuration, directly obtaining photovoltaic  $J$ - $V$  curves. Fig. S18† shows the  $J$ - $V$  characteristics of the  $\text{Cu}_2\text{O}/\text{Ga}_2\text{O}_3/\text{TiO}_2$  DWE device before and after a stability measurement that was carried out at short circuit for 2 h, where an obvious  $V_{\text{oc}}$  decrease in a range of 100 mV was observed. Since corrosion through any pinholes in the ALD protective layer can be ruled out in the solid state measurement, we attribute the loss of the PEC performance in this system to an intrinsic problem with the  $\text{Cu}_2\text{O}/\text{Ga}_2\text{O}_3$  junction. Further studies are underway to more clearly identify the underlying reason for the instability of this junction.

## Conclusions

We have developed a new configuration of the DWE technique that is able to probe the surface potential of a water splitting photocathode under operation without interfering in the charge transfer processes at the different interfaces in actual water splitting PEC devices. Although we have focused on ALD  $\text{TiO}_2$  in this work due to its widespread use, we expect that our DWE architecture is applicable to other overlayer materials as well, provided they are sufficiently conductive, which is a requirement for PEC electrodes in any case.<sup>28</sup> This technique has been demonstrated as a universal method to systematically investigate independently the photovoltaic and electrocatalytic properties of catalyst-modified buried junction photocathodes. A



Fig. 4 (a) Schematic structure of a  $\text{Cu}_2\text{O}/\text{Ga}_2\text{O}_3/\text{TiO}_2/\text{Pt}(\text{sp})$  photocathode. The thickness of  $\text{Ga}_2\text{O}_3$  and  $\text{TiO}_2$  ALD-layers are 20 and 100 nm, respectively. WE1 controls the back contact potential  $V_1$  and WE2 measures the surface potential  $V_2$ . (b)  $J$ - $\Delta V$  curves (dashed) of  $\text{Cu}_2\text{O}/\text{Ga}_2\text{O}_3/\text{TiO}_2/\text{Pt}(\text{sp})$  before and after 2 h stability test, overlaid with the corresponding  $J$ - $V_1$  curves (solid).



pn<sup>+</sup>Si/TiO<sub>2</sub>/Pt photocathode was first fabricated as a platform to model the DWE system. By means of surface potential measurements, the intrinsic properties of the buried p-n junction were studied, and the hidden *J*-*V* curve of a photovoltaic cell was extracted. Additionally, the fill factor loss between *J*-*V*1 and *J*-Δ*V* curves was identified as a parameter that characterizes the TiO<sub>2</sub>/Pt/electrolyte interface, where the morphology of the catalyst plays an important role. Furthermore, the PEC performance degradation mechanism was investigated and discussed. We have demonstrated that the stability of underlying p-n junctions in buried junction photocathodes can be characterized under *operando* conditions. Finally, we applied the DWE technique to a promising emerging system based on Cu<sub>2</sub>O/Ga<sub>2</sub>O<sub>3</sub>, where it was found that the large photovoltage decreases over time. The degradation in the photovoltage with time was also observed in the solid state, ruling out any potential corrosion by the electrolyte. As new material combinations are synthesized for PEC measurements, the DWE electrode technique enables a rapid diagnosis of the cause of degradation in these systems, while also obtaining the PV characteristics of these newly developed junctions without the need to construct separate PV cells.

## Conflicts of interest

There are no conflicts to declare.

## Acknowledgements

The University of Zurich, the University Research Priority Program (URPP) LightChEC, and the Swiss National Science foundation (AP Energy Grant # PYAPP2 160586) are gratefully acknowledged for financial support. Wenzhe Niu thanks Zhejiang University for an international study and communication fellowship. The authors acknowledge the assistance and support of the Center for Microscopy and Image Analysis at the University of Zurich for the SEM characterization. The authors would also like to thank Dr Olivier Blacque (Department of Chemistry, University of Zurich) for his assistance in the XRD characterization.

## References

- 1 A. Heller, *Science*, 1984, **223**, 1141–1148.
- 2 M. Gratzel, *Nature*, 2001, **414**, 338–344.
- 3 E. L. Miller, *Energy Environ. Sci.*, 2015, **8**, 1809.
- 4 M. S. Prévot and K. Sivula, *J. Phys. Chem. C*, 2013, **117**, 17879–17893.
- 5 Y. Nakato, Y. Egi, M. Hiramoto and H. Tsubomura, *J. Phys. Chem.*, 1984, **88**, 4218–4222.
- 6 S. W. Boettcher, E. L. Warren, M. C. Putnam, E. A. Santori, D. Turner-Evans, M. D. Kelzenberg, M. G. Walter, J. R. McKone, B. S. Brunschwig, H. A. Atwater and N. S. Lewis, *J. Am. Chem. Soc.*, 2011, **133**, 1216–1219.
- 7 Q. Huang, Z. Ye and X. Xiao, *J. Mater. Chem. A*, 2015, **3**, 15824–15837.
- 8 T. Hisatomi, J. Kubota and K. Domen, *Chem. Soc. Rev.*, 2014, **43**, 7520–7535.
- 9 Z. Zhang and J. T. Yates, *Chem. Rev.*, 2012, **112**, 5520–5551.
- 10 T. A. Pham, Y. Ping and G. Galli, *Nat. Mater.*, 2017, **1**–8.
- 11 Y. Nakato, T. Ohnishi and H. Tsubomura, *Chem. Lett.*, 1975, **4**, 883–886.
- 12 W. E. Pinson, *Nature*, 1977, **269**, 316–318.
- 13 R. Wilson, L. Harris and M. Gerstner, *J. Electrochem. Soc.*, 1977, **124**, 2–3.
- 14 F. Lin and S. W. Boettcher, *Nat. Mater.*, 2013, **13**, 81–86.
- 15 G. Hodes, L. Thompson, J. Dubow and K. Rajeshwar, *J. Am. Chem. Soc.*, 1983, **1289**, 324–330.
- 16 J. R. White, F.-R. F. Fan and A. J. Bard, *J. Electrochem. Soc.*, 1985, **132**, 544–550.
- 17 B. Seger, T. Pedersen, A. B. Laursen, P. C. K. Vesborg, O. Hansen and I. Chorkendorff, *J. Am. Chem. Soc.*, 2013, **135**, 1057–1064.
- 18 J. Gu, Y. Yan, J. L. Young, K. X. Steirer, N. R. Neale and J. a. Turner, *Nat. Mater.*, 2015, **15**, 456.
- 19 W. Septina, R. R. Prabhakar, R. Wick, T. Moehl and S. D. Tilley, *Chem. Mater.*, 2017, **29**, 1735–1743.
- 20 K. T. Fountaine, H. J. Lewerenz and H. A. Atwater, *Nat. Commun.*, 2016, **7**, 13706.
- 21 B. Seger, D. S. Tilley, T. Pedersen, P. C. K. Vesborg, O. Hansen, M. Gratzel and I. Chorkendorff, *RSC Adv.*, 2013, **3**, 25902–25907.
- 22 A. Paracchino, V. Laporte, K. Sivula, M. Gratzel and E. Thimsen, *Nat. Mater.*, 2011, **10**, 456–461.
- 23 E. Kemppainen, A. Bodin, B. Sebok, T. Pedersen, B. Seger, B. Mei, D. Bae, P. C. K. Vesborg, J. Halme, O. Hansen, P. D. Lund and I. Chorkendorff, *Energy Environ. Sci.*, 2015, **8**, 2991–2999.
- 24 A. Paracchino, N. Mathews, T. Hisatomi, M. Stefik, S. D. Tilley and M. Graetzel, *Energy Environ. Sci.*, 2012, **5**, 8673–8681.
- 25 C. Li, T. Hisatomi, O. Watanabe, M. Nakabayashi, N. Shibata, K. Domen and J.-J. Delaunay, *Energy Environ. Sci.*, 2015, **8**, 1493–1500.
- 26 Y. S. Lee, D. Chua, R. E. Brandt, S. C. Siah, J. V Li, J. P. Mailoa, S. W. Lee, R. G. Gordon and T. Buonassisi, *Adv. Mater.*, 2014, **26**, 4704–4710.
- 27 T. Minami, Y. Nishi and T. Miyata, *Appl. Phys. Express*, 2013, **6**, 44101.
- 28 J. Azevedo, S. D. Tilley, M. Schreier, M. Stefik, C. Sousa, J. P. Araújo, A. Mendes, M. Grätzel and M. T. Mayer, *Nano Energy*, 2016, **24**, 10–16.

